PAPER

Application of Wavelets to Scattering Problems of Inhomogeneous Dielectric Slabs

Jeng-Long LEOU[†], **Jiunn-Ming HUANG**[††], **Shyh-Kang JENG**[†††], *and* **Hsueh-Jyh LI**[†††], ***Nonmembers***

SUMMARY In this paper, we apply the discrete wavelet transform (DWT) and the discrete wavelet packet transform (DWPT) with the Daubechies wavelet of order 16 to effectively solve for the electromagnetic scattering from a one-dimensional inhomogeneous slab. Methods based on the excitation vector and the $[\boldsymbol{Z}]$ matrix are utilized to sparsify an MoM matrix. As we observed, there are no much high frequency components of the field in the dielectric region, hence the wavelet coefficients of the small scales components (high frequency components) are very small and negligible. This is different from the case of two-dimensional scattering from perfect conducting objects. In the excitation-vector-based method, a modified excitation vector is introduced to extract dominant terms and achieve a better compression ratio of the matrix. However, a smaller compression ratio and a tiny relative error are not obtained simultaneously owing to their deletion of interaction between different scales. Hence, it is inferior to the $[\boldsymbol{Z}]$-matrix-based methods. For the $[\boldsymbol{Z}]$-marix-based methods, our numerical results show the column-tree-based DWPT method is a better choice to sparsify the MoM matrix than DWT-based and other DWPT-based methods. The cost of a matrix-vector multiplication for the wavelet-domain sparse matrix is reduced by a factor of 10, compared with that of the original dense matrix.

key words: *wavelets, scattering, method of moment, integral equations*

1. Introduction

The wavelet theory has been widely employed to solve the integral equations in electromagnetic field problems [1]–[11]. The solution, in general, can be divided into two categories. The first one is to obtain a matrix equation by the method of moment (MoM), where the matrix elements are calculated using wavelets as basis functions [1]–[4]. The other is to form the MoM matrix equation by conventional basis functions first, then apply the wavelet transform to get a new matrix equation (similarity transform approach) [5]–[11]. Both methods will result in sparse matrix equations, which can be solved with less memory and computation time. In order to increase the sparsity of matrix in the similarity transform approach, researchers have applied different wavelet theories such as discrete wavelet transform (DWT) [5] and discrete wavelet packet transform (DWPT) [6]–[8] to transform the original MoM matrix equations. Before using the DWPT in the similarity transform approach, several authors developed the best base selection algorithms [12], [13] to search for a more suitable basis for near optimal sparsity [6]–[8]. Some authors also used the physical characteristics of the problem to extract the dominant wavelet bases and solve a smaller system of linear equation [9], [10].

The works mentioned above are all concentrated on the scattering of perfect electric conducting (PEC) objects. Nevertheless, problems of dielectric objects are also important, and up to now no published literature addressed on applying wavelet techniques to dielectric scattering problems. For such problems the number of unknowns are much more than that of a PEC object scattering problem. Thus, matrix sparsification is even more valuable in solving this kind of problem. In this paper, we will apply various similarity transform methods to the scattering of one dimensional slabs and determine which one will make the best sparsity.

This paper is organized as follows. First, in Sect. 2 we state the problem of scattering from one dimensional dielectric slab. A brief review of the similarity transform approach using the DWT or the DWPT is given in Sect. 3. Three popular methods, the excitation-based method, the $[\boldsymbol{Z}]$-matrix-based method and the hybrid method are also presented in Sect. 3. In Sect. 4, numerical results of these three methods are exhibited and discussed. Finally, conclusions are made in Sect. 5.

2. Statement of Problem

Consider a uniform plane wave normally incident on an inhomogeneous dielectric slab (Fig. 1). For simplicity, only the TM case is considered. The integral equation of this scattering problem can be derived as [14]

$$E(x) + \int_0^L K(x, x')E(x')\,dx' = E^i(x) \tag{1}$$

where

Manuscript received November 2, 1998.
Manuscript revised March 8, 1999.

[†]The author is with the Department of Electrical Engineering, National Taiwan University, Taiwan, Republic of China.
[††]The author is with the Department of Communication Engineering, National Chiao-Tung University Hsinchu, Taiwan, Republic of China.
[†††]The authors are with the Department of Electrical Engineering and Graduate Institute of Communication Engineering, National Taiwan University, Taiwan, Republic of China.

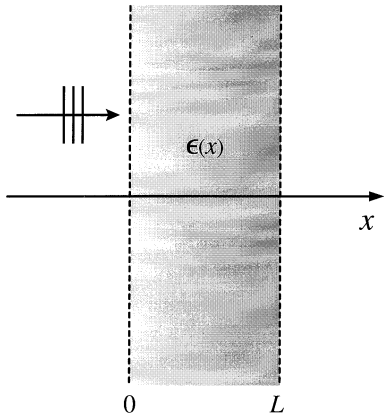

Fig. 1 Scattering from a one-dimensional inhomogeneous slab.

$$K(x,x') = \frac{jk_o}{2} e^{-jk_o|x-x'|} \cdot [\epsilon(x') - 1] \quad 0 \le x, x' \le L \tag{2}$$

L is the thickness of the slab, $\epsilon(x')$ is the distribution of the dielectric constant in the slab, k_o is the wavenumber in free space, $E(x)$ and $E^i(x)$ are the total field and incident field respectively. Here a time dependence of $e^{j\omega t}$ is assumed and suppressed throughout this paper.

In solving Eq. (1), the total field $E(x)$ can be expanded by pulse basis functions, and the point matching can be applied to Eq. (1) to obtain a matrix equation [15]

$$[\boldsymbol{Z}]\boldsymbol{x} = \boldsymbol{b} \tag{3}$$

Note that this matrix equation is the same as that derived for PEC objects, but the kernel $K(x,x')$ and thus the $[\boldsymbol{Z}]$ matrix in (3) depends on the dielectric constant distribution, which is different from the PEC case.

3. Similarity Transform and Sparsification

After forming the matrix equation (3) by conventional basis functions, two similarity transform matrices , $[W_e]$ and $[W_t]$, are used to change the original expansion and testing functions into a new set of expansion and testing functions, respectively. The columns of $[W_e]$ and $[W_t]$ consist of the wavelet bases. Using $[W_e]$ and $[W_t]$, we obtain a new matrix equation in the wavelet scale domain

$$[\tilde{\boldsymbol{Z}}]\tilde{\boldsymbol{x}} = \tilde{\boldsymbol{b}} \tag{4}$$

where

$$\tilde{\boldsymbol{x}} = [W_e]^T \boldsymbol{x} \tag{5}$$

$$\tilde{\boldsymbol{b}} = [W_t]^T \boldsymbol{b} \tag{6}$$

$$[\tilde{\boldsymbol{Z}}] = [W_t]^T [\boldsymbol{Z}] [W_e] \tag{7}$$

Here T denotes the transpose of a matrix and $\sim$ denotes the representation in the wavelet domain.

The forms of $[W_e]$ and $[W_t]$ depend on the choice of wavelet transform methods and the sparsification techniques. In general, there are two kinds of wavelet transforms: the discrete wavelet transform (DWT) [16] and the discrete wavelet packet transform (DWPT) [12]. Because that the DWT is a special case of the DWPT, we discuss the DWPT first. While applying the DWPT, we have to select the packet tree for the matrix equation. Two categories of packet tree selection can be used. The first one analyzes the best bases based on the excitation $\boldsymbol{b}$, and leads to $[W_e] = [W_t]$ using the same wavelet bases. The other searches for the best packet tree associated with the $[\boldsymbol{Z}]$ matrix. The $[W_e]$ and $[W_t]$ are determined by processing the rows and columns of the $[\boldsymbol{Z}]$ matrix, respectively. If we apply the DWT instead, the packet tree is automatically generated in the DWT algorithm, which results in $[W_e] = [W_t]$. For details of the DWT and the DWPT, see [12], [16].

Three popular methods are applied in order to sparsify or reduce the matrix equation. The first one reduces the size of matrix equation based on the dominant terms of the excitation vector, but the reduced matrix is full [9], [10]. It is called the excitation-based method. The second method, the $[\boldsymbol{Z}]$-matrix-based method, keeps the matrix dimension and the matrix becomes sparse after a thresholding procedure [5], [7], [8], [11]. The third one is a hybrid method, which is similar to the first method but with a sparse matrix of the same size [6]. If the DWT is applied with these three methods, the hybrid method is the same as the $[\boldsymbol{Z}]$-matrix-based method.

In this work, we implement the DWT and the DWPT along with the three sparsification techniques to the scattering of one dimensional slabs. The procedure is listed as follows.

1. Discretize the integral equation to a matrix equation $[\boldsymbol{Z}]\boldsymbol{x} = \boldsymbol{b}$.
2. Apply the DWT or the DWPT to the matrix equation.
   (a) Suppose that the excitation-based method is preferred.
      i. Apply the DWT or the DWPT to the excitation vector. If the DWPT is adopted, perform the best packet tree selection to the excitation vector $\boldsymbol{b}$ and get a best packet tree. If the DWT is used, the packet tree selection is skipped.
      ii. Extract the dominant terms from $\tilde{\boldsymbol{b}}$ and determine the transform matrices $[W] = [W_e] = [W_t]$.
      iii. Transform the matrix equation into the wavelet domain with a reduced size.
   (b) Assume that the $[\boldsymbol{Z}]$-matrix-based method is

employed.

i. Apply the DWT to the matrix equation with $[W] = [W_e] = [W_t]$. Or apply the DWPT to the rows and columns of $[\boldsymbol{Z}]$ matrix to determine the best packet trees, then decide the transform matrices $[W_e]$ and $[W_t]$ according to the best packet trees.
ii. Transform the matrix equation into the wavelet domain.
iii. Sparsify the transformed matrix by certain thresholding techniques.

(c) If the hybrid method is utilized [6], apply the DWPT to the $[\boldsymbol{Z}]$ matrix according to the best packet tree determined by the excitation vector. And then use certain thresholding techniques to sparsify the transformed matrix.

3. Solve the wavelet-based matrix equation $[\tilde{\boldsymbol{Z}}]\tilde{\boldsymbol{x}} = \tilde{\boldsymbol{b}}$.
4. Take the inverse DWT or DWPT of $\tilde{\boldsymbol{x}}$ to obtain the approximate solution $\boldsymbol{x}_{comp}$.

4. Numerical Results and Discussions

In this section we present some numerical examples for different dielectric profiles. The profiles include the small-variation profile $\epsilon_1(x)$, the linearly-decreasing profile $\epsilon_2(x)$ and the abruptly-changing profile $\epsilon_3(x)$:

$$\epsilon_1(x) = \epsilon_b + A + A\sin\left(2\pi\frac{x}{L}\right) \tag{8}$$

$$\epsilon_2(x) = 1 + (\epsilon_m - 1)\left(1 - \frac{x}{L}\right) \tag{9}$$

$$\epsilon_3(x) = \begin{cases} 10 & x \in \left[0, \dfrac{L}{3}\right) \cup \left[\dfrac{2L}{3}, L\right] \\ 1 & x \in \left[\dfrac{L}{3}, \dfrac{2L}{3}\right) \end{cases} \tag{10}$$

where $A = 0.1$, $\epsilon_b = 1$–10 and $\epsilon_m = 10$ are the amplitude of dielectric variation, the background dielectric constant and the maximum relative dielectric constant, respectively.

Collocation method with pulse basis is then employed to form the MoM matrix equation. By changing the slab thickness L/λ_o and fixing the pulse width $\Delta = \lambda_o/32$, we obtain the moment matrices with sizes ranging from $N = 128$ to 2048. All methods described in the last section are applied to sparsify or reduce the size of the matrix equation.

Although various families of wavelet bases have been developed [17], [18], we only consider the periodic Daubechies wavelet of order 16 (vanishing moments = 8). The behavior of such a wavelet basis is good enough to approximate the smooth $E(x)$ field inside the slab. When the DWPT is applied, a commonly used cost function, the additive energy concentration function with $p = 1$ [12], [13], and the "top-down" tree search algorithm are utilized.

One parameter to measure the sparseness of a matrix is the compression ratio. Here we define the compression ratio ρ as the ratio of the number of non-zero elements N_{nz} to the size of the original dense matrix N^2.

$$\rho = \frac{N_{nz}}{N^2} \times 100\% \tag{11}$$

Additionally, as a measure of the solution accuracy, the relative residual error is defined as

$$E_{err} = \frac{||\boldsymbol{x} - \boldsymbol{x}_{comp}||}{||\boldsymbol{x}||} \times 100\% \tag{12}$$

where $\boldsymbol{x}$, $\boldsymbol{x}_{comp}$ are the original MoM solution and our computed approximate solution, respectively.

4.1 Excitation-Based Method

The objective of the excitation-based method is to find a best reference vector to represent the dominant terms of the total field in the wavelet domain. Most previous works dealt with the PEC scattering problems, and used the incident field as the reference (excitation) vector [9], [10]. In our study, we introduce a modified reference vector $\boldsymbol{b}_m$ to estimate the dominant terms in the wavelet domain more precisely. We define

$$\boldsymbol{b}_m = e^{-jk_o\sqrt{\epsilon_s(x)}\,x} \tag{13}$$

where the selection of $\epsilon_s(x)$ depends on the dielectric profiles. For the small-variation profiles and the linearly-decreasing profile, we choose $\epsilon_s(x) = \epsilon_b$ and $\epsilon_s(x) = \overline{\epsilon_2(x)}$, respectively. Where $\overline{\epsilon_2(x)}$ is the average of $\epsilon_2(x)$. For the abruptly-changing profile, we tried several forms of the modified reference vectors but their performance are not satisfactory. For the other two profiles, reference vectors defined by (13) can reflect the characteristics of the dielectric profiles, so we may expect the dominant terms determined this way are closer to the dominant parts of the total field in the wavelet domain. This can be observed from the discussions of Fig. 2 and examples below. Moreover, the excitation-based method can be applied along with the DWT or the DWPT technique. In the results given in this section, Figures 2–5 and Figures 6, 7 are computed via the DWT and the DWPT, respectively.

In Fig. 2, the normalized wavelet domain coefficients, $\tilde{\boldsymbol{x}}$, $\tilde{\boldsymbol{b}}$ and $\tilde{\boldsymbol{b}}_m$, are compared for the small-variation profile with $\epsilon_b = 10$. The dotted, dashed and solid lines stand for $\tilde{\boldsymbol{x}}$, $\tilde{\boldsymbol{b}}$ and $\tilde{\boldsymbol{b}}_m$, respectively. It is seen that $\tilde{\boldsymbol{b}}$ and $\tilde{\boldsymbol{b}}_m$ are much different and $\tilde{\boldsymbol{b}}_m$ is closer to $\tilde{\boldsymbol{x}}$ than $\tilde{\boldsymbol{b}}$ is. We can expect that the modified reference vector (13) can give a more precise dominant-term (the

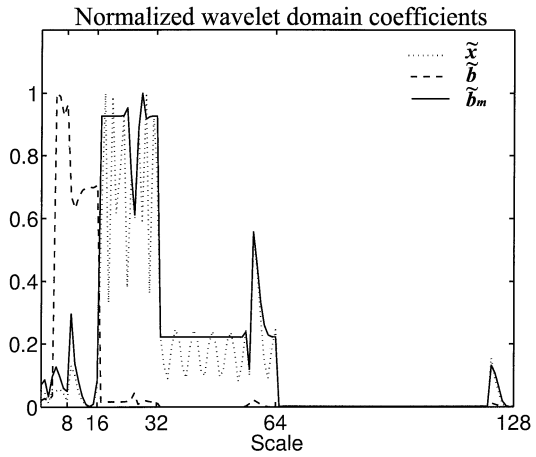

Fig. 2 The normalized wavelet domain coefficients, $\tilde{\boldsymbol{x}}$, $\tilde{\boldsymbol{b}}$ and $\tilde{\boldsymbol{b}}_m$, for the small-variation profile with $N = 128$, $A = 0.1$ and $\epsilon_b = 10$.

peaks in Fig. 2) prediction.

Besides, according to our experience, the profiles of wavelet coefficients (the energy distribution) move toward to the small scale region as ϵ_b increase from 1 to 10. The reason is that a high dielectric constant will result in a small equivalent wavelength in the space domain, which is corresponding to small scale coefficients in the wavelet domain. In addition, the wavelet coefficients are negligible in the small scale region. After extracting the dominant components in the large scale part, we obtain a smaller matrix equation. Note that the wavelet scale decreases as the number labeled on the horizontal axis increases in Fig. 2.

Figure 3 illustrates the variation of compression ratio ρ with respect to the relative error E_{err} for $\epsilon_1(x)$ with $\epsilon_b = 10$ of various $N = 256$, 512 and 1024. Figures 3(a) and (b) are the results for $\boldsymbol{b}$ and $\boldsymbol{b}_m$, respectively. It is seen that the compression ratio are improved if $\boldsymbol{b}_m$ is used as reference vector. A sharp change of relative error nearby $20\% < \rho < 30\%$ is also discovered in Fig. 3. It can be explained from Fig. 2: Almost half of the wavelet coefficients are near zero, hence its corresponding compression ratio is about $\rho = \frac{(N/2)^2}{N^2} \times 100 = 25\%$. It gives an estimation of the upper bound of the compression ratio for this method, when the relative error is not too large.

The curves of the compression ratio ρ of matrix $[\tilde{\boldsymbol{Z}}]$ for the linearly-decreasing profile $\epsilon_2(x)$ are shown in Fig. 4. Only the results using the reference vector $\boldsymbol{b}$ are illustrated because the results of $\boldsymbol{b}_m$ are similar. The compression ratio for different discretization size $N = 128$, 512 and 2048 are compared. Here we also see that the relative error rises as N increases. It is noted that the curves of compression ratio do not change too much when N changes. This means that there is no significant improvement of the compression ratio for large N, and this will be not useful for large N of dielectric

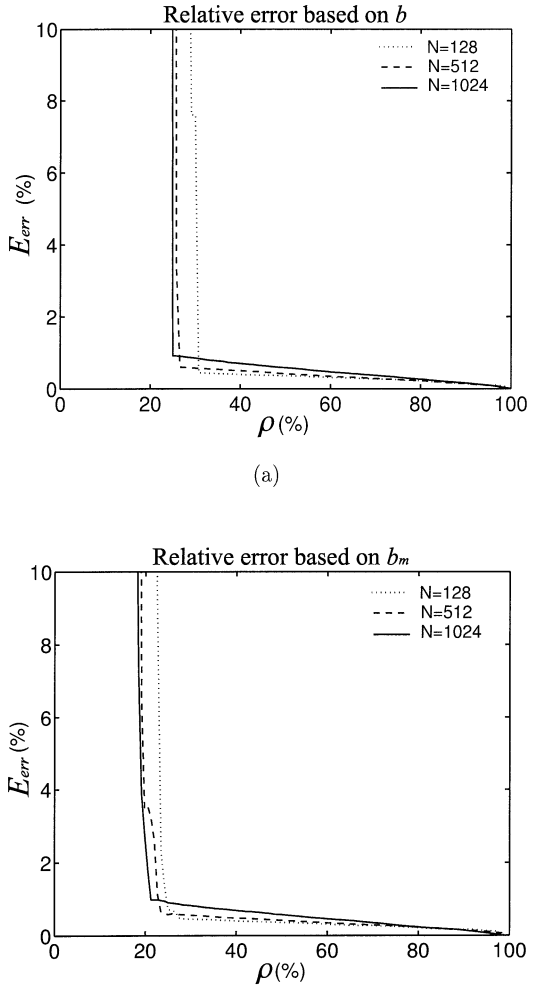

Fig. 3 Relative error versus the compression ratio of MoM matrices. Cases shown are for the small-variation profile with $\epsilon_b = 10$ of various $N = 128$, 512 and 1024. (a) Using $\boldsymbol{b}$ (b) using $\boldsymbol{b}_m$.

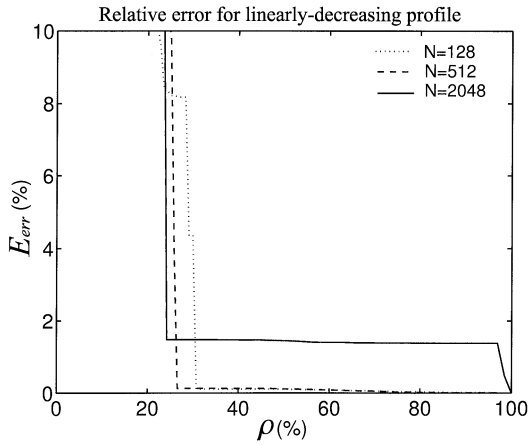

Fig. 4 Relative error versus the compression ratio of MoM matrices. Cases shown are for the linearly-decreasing profile of various problem size $N = 128$, 512 and 2048.

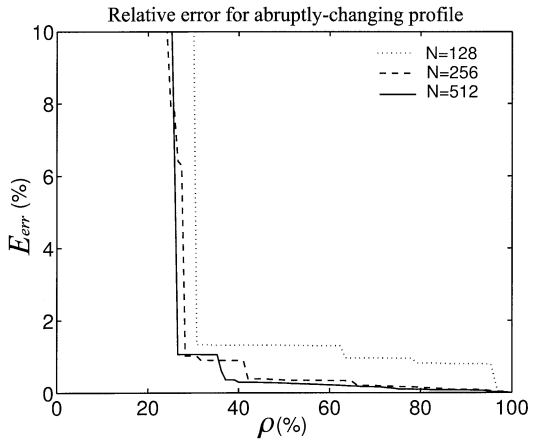

Fig. 5 Relative error versus the compression ratio of MoM matrices. Cases shown are for the abruptly-changing profile of various problem size, $N = 128$, 256 and 512.

slabs.

For the abruptly-changing profile $\epsilon_3(x)$, the curves of compression ratio ρ of matrix $[\tilde{\boldsymbol{Z}}]$ for $N = 128$, 256 and 512 are shown in Fig. 5. There is no significant difference as for the case of $\epsilon_1(x)$. For larger N, the relative errors are smaller before the abrupt turning points. It also shows that at least 25% compression ratio can be achieved as in Figs. 3 and 4.

Similar experiments were also carried out by using the DWPT. If $\boldsymbol{b}$ is used, only one packet tree has to be determined for each N. Various profiles can use the same result without researching the packet tree again. On the other hand, if $\boldsymbol{b}_m$ is utilized, we have to search the packet tree for each N and different dielectric profile.

The DWPT trees for both $\boldsymbol{b}$ and $\boldsymbol{b}_m$ of $N = 128$ in the case of linearly-decreasing profile are shown in Fig. 6, where $\epsilon_s = 5.5$ is chosen for $\boldsymbol{b}_m$. Both of them do not level off until the decomposition procedures reach the final level. The packet tree of $\boldsymbol{b}$ branches more than that of $\boldsymbol{b}_m$ does, because $\boldsymbol{b}$ contains less information. In general, a tree with many branches implies an ineffective decomposition.

The curves of compression ratio for the linearly-decreasing profile by using reference vector $\boldsymbol{b}$ and $\boldsymbol{b}_m$ for matrices of $N = 128$ and 256 are shown in Fig. 7. The results of modified reference vector $\boldsymbol{b}_m$ are better than those of $\boldsymbol{b}$. Contrary to the trend in Figs. 3, 4 and 5, the compression ratio of matrices are not improved when N increases. This can be explained as follows: The number of branches of the packet trees of $\boldsymbol{b}$ and $\boldsymbol{b}_m$ increases with N. More tree branches means that there is no important information in the reference vectors. Extra branches can generate more errors in reducing the matrix equation after the packet tree being constructed. This makes the compression ratio worse.

From the point of view of matrix compression, the

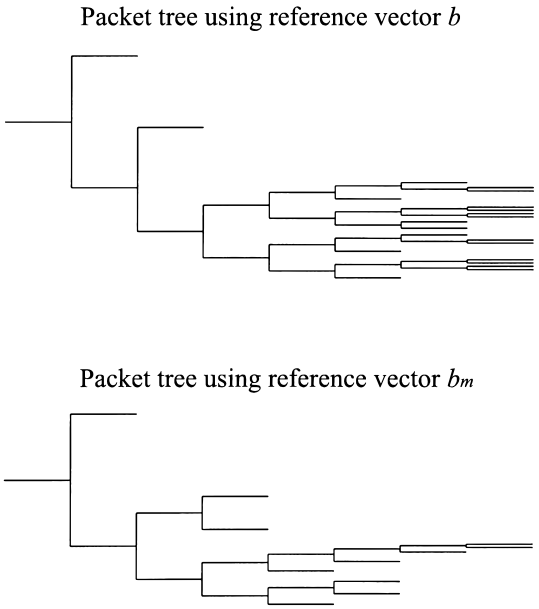

Fig. 6 Packet trees referred to the vectors $\boldsymbol{b}$ and $\boldsymbol{b}_m$. Cases are shown for $N = 128$ and $\epsilon_s(x) = 5.5$ for $\boldsymbol{b}_m$.

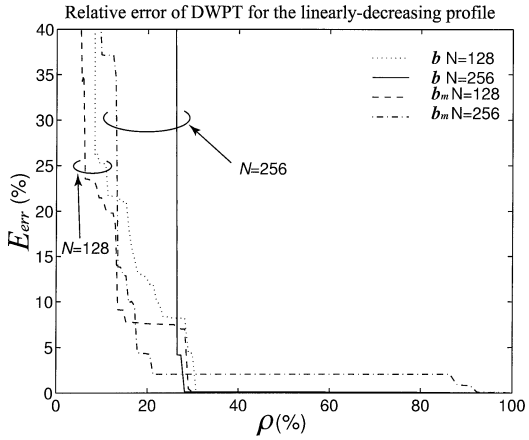

Fig. 7 Relative error versus the compression ratio of MoM matrix. Cases shown are for the linearly-decreasing profile of $N = 128$ and 256 by using the excitation-based method with DWPT.

excitation-based method can produce satisfactory results to some degrees for this kind of problems. But it is not good if a more precise result as well as a smaller compression ratio are requested. Noted from the above examples, the compression ratio is not easy to reach 20% even when the relative error is over 10%. Since only one excitation vector is used, it can not contain too much physical information to predict the dominant terms [6], [9]. Moreover, while reducing the MoM matrix, the elements which contain the interaction between different scales are deleted. The deletion of these elements may lead to inaccurate results. On the contrary, $[\boldsymbol{Z}]$-matrix-based algorithm retains all scales in

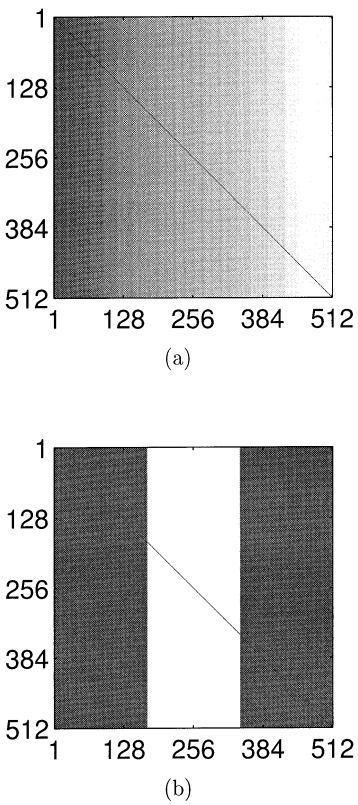

Fig. 8 The original MoM matrix of (a)the linearly-decreasing profile, (b) the abruptly-changing profile.

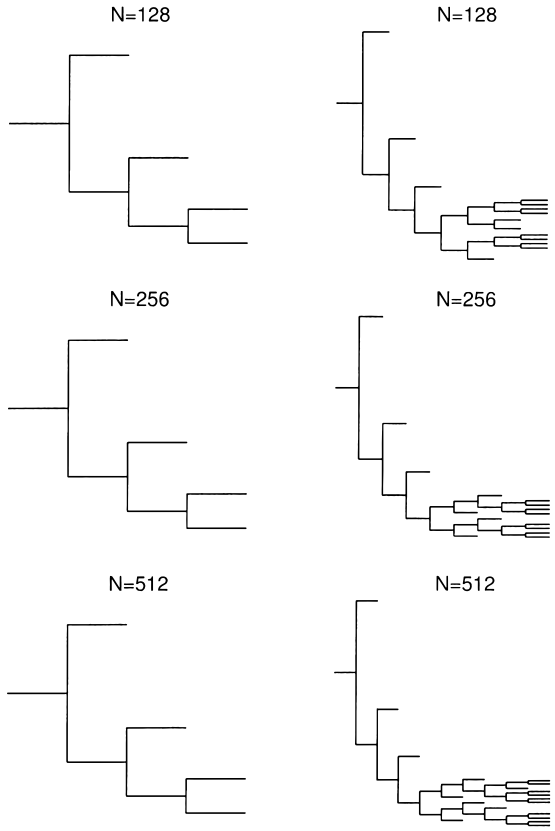

Fig. 9 The packet trees by searching within columns and rows of the MoM matrix. Cases are shown for the linearly-decreasing profile of various $N = 128$, 256 and 512.

the wavelet domain and thus the interaction between different scales are preserved. Better compression ratio can be obtained even a small E_{err} is requested. Hence, the results in the next subsection will compare the compression ratio for a much smaller fixed E_{err} with various N.

4.2 [$\boldsymbol{Z}$]-matrix-Based Algorithms and Hybrid Methods

In this subsection, the [$\boldsymbol{Z}$]-matrix-based methods are discussed. To study the relationship between the matrix size N and the matrix sparsity for a fixed solution accuracy, we computed the case of the linearly-decreasing profile $\epsilon_2(x)$ and the abruptly-changing profile $\epsilon_3(x)$ with an increasing size, with the element threshold adjusted to maintain a relative error $E_{err} = (1\pm0.02)\%$. The discretization density is kept at $\lambda_o/32$, and the results obtained by using the DWT, the DWPT and the hybrid method are all used and compared. The case of $\epsilon_1(x)$ is not considered because it is similar to the results of $\epsilon_2(x)$.

Figure 8 shows the magnitude of the elements of original MoM [$\boldsymbol{Z}$] matrices of $\epsilon_2(x)$ and $\epsilon_3(x)$ for $N = 512$. It is seen that the MoM matrices contain the information of the dielectric constant distribution, and are nonsymmetric. The packet trees of expansion functions and testing functions by dealing with the rows and columns of these two matrices with $N = 128$, 256 and 512 are shown in Figs. 9 and 10 for $\epsilon_2(x)$ and $\epsilon_3(x)$, respectively. As the figures indicate, the trees obtained from rows (row tree, left column in Figs. 9 and 10) branch out only three levels and identical to the first three levels of the standard DWT; while for the trees corresponding to the columns (column tree, right column in Figs. 9 and 10), the branch can not level off until the final level, and note that first four levels of decomposition in both cases are identical to the DWT results. We expect that the additional sparsity obtained in DWPT comes from decomposition levels larger than four. Furthermore, the difference between the row tree and the column tree can be explained by investigating the elements of the [$\boldsymbol{Z}$] matrix in Fig. 8. The row elements of the MoM matrices vary with the spatial distribution of the dielectric constant, hence the rows contain more information and the related branches level off quickly. Note that it does not imply that less decomposition levels of packet tree will result in a superior matrix compression ratio.

Figures 11 and 12 illustrate the sparseness structures of the transformed MoM matrices of $\epsilon_2(x)$ and $\epsilon_3(x)$ by using the DWT, the DWPT based on the excitation vector, the DWPT based on the row tree,

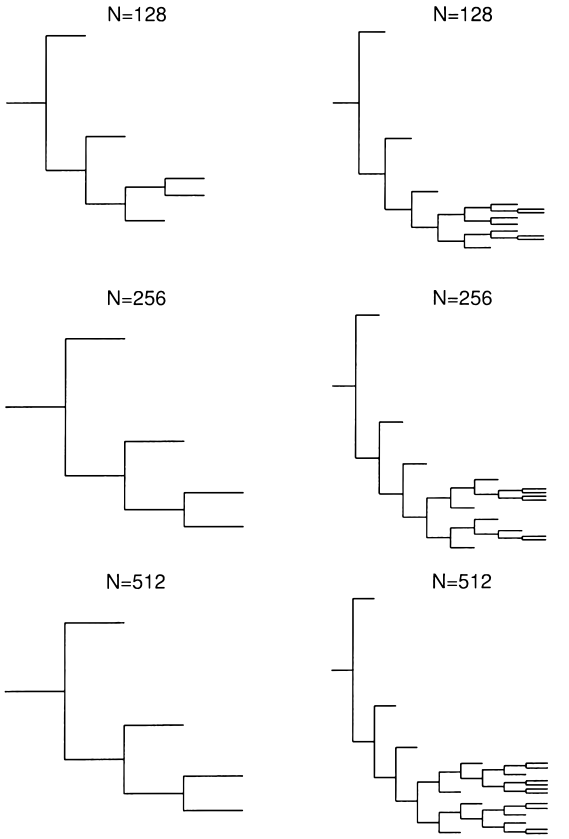

Fig. 10 The packet trees by searching within columns and rows of the MoM matrix. Cases are shown for the abruptly-changing profile of various $N = 128$, 256 and 512.

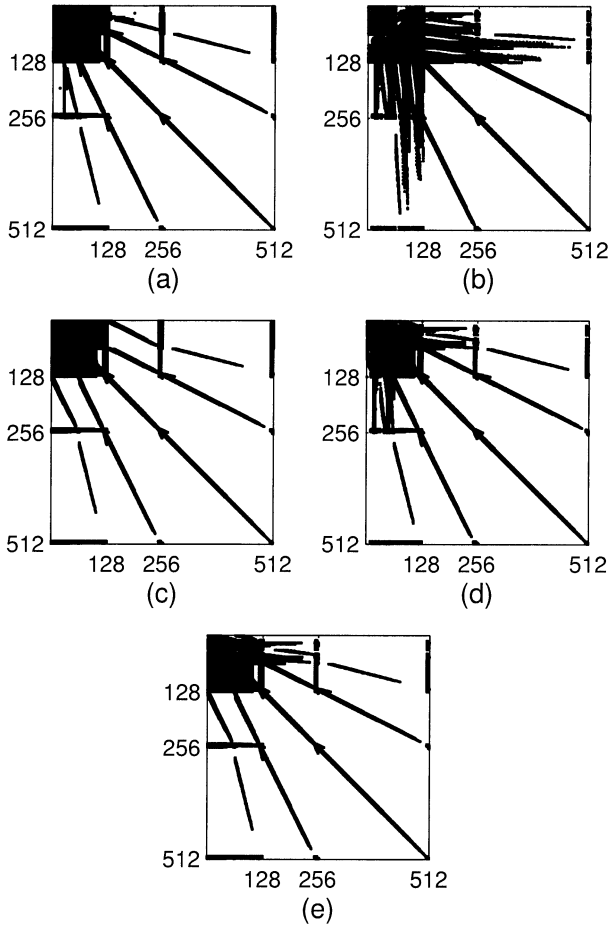

Fig. 11 The transformed moment matrices of the linearly-decreasing profile with $N = 512$ after thresholding procedure using (a) the DWT, (b) the DWPT based on the excitation tree, (c) the DWPT based on the row tree, (d) the DWPT based on the column tree, and (e) the DWPT based on the column-row tree.

the DWPT based on the column tree, and the DWPT based on the column-and-row tree for $N = 512$ with $E_{err} = (1 \pm 0.02)\%$. The vertical and horizontal fingers around power of 2 (e.g. 256 and 512) are due to the periodic nature of the wavelet basis, and different packet bases applied to the rows and columns of MoM matrices result in different sparseness structures of the transformed matrices. The major difference between the sparseness structures of these methods are in the large-scale region (left-upper region). It is corresponding to the lower decomposition level. Which kind of packet bases are better to sparsify the MoM matrices are examined below.

The results of compression ratio versus the problem size for the linearly-decreasing profile are presented in Fig. 13. All methods mentioned in last paragraph are applied and compared. It is seen that DWT-produced sparsities (dotted line) level off faster than the others for large N, and the DWPT based on the column tree (dotted line with circle) are superior among these method. It can be explained as follows: As we mentioned previously, less tree decomposition level does not imply a sparser matrix for a given E_{err}, because more decompositions will result in more complete basis functions. Hence, the results of the DWPT based on the column tree are better than others. In addition, packet tree selection based on the excitation vector is also a good choice to sparsify the MoM matrix (dashdot line) owing to the small cost for packet tree selection.

Figure 14 presents the sparsity for the abruptly-changing profile. Here we see that the results based on the row tree are worse than the others, because the total field distribution of this case is more complicated than the results of $\epsilon_2(x)$, and the decomposition level of the row tree is not enough to approximate the total filed in the slab region.

Figures 15 and 16 compare the CPU times required for a single matrix-vector multiplication (MVM) as a function of N, using the DWT and the DWPT based on both the $[\boldsymbol{Z}]$-matrix-based methods and the hybrid method. The results of the original dense matrix are also plotted for reference (dotted line). All the computation was performed on a pentium II 300 MHz PC with 256 MB RAM using MATLAB and a fixed

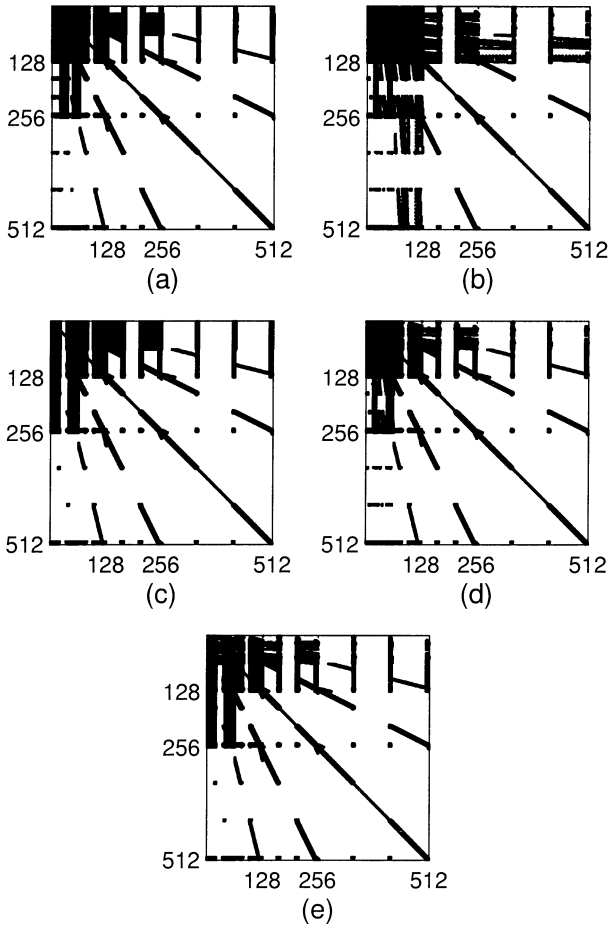

Fig. 12 The transformed moment matrices of the abruptly-changing profile with $N = 512$ after thresholding procedure using (a) the DWT, (b) the DWPT based on the excitation tree, (c) the DWPT based on the row tree, (d) the DWPT based on the column tree, and (e) the DWPT based on the column-row tree.

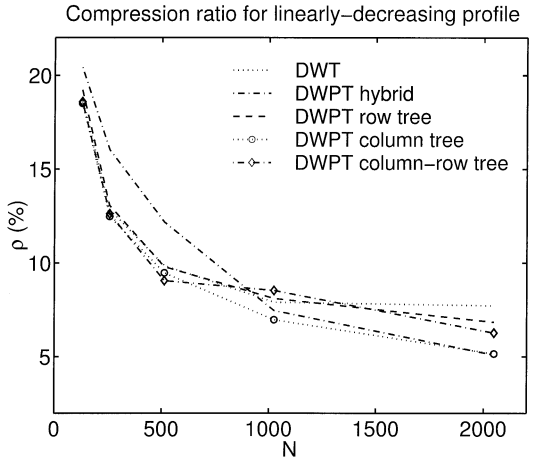

Fig. 13 The compression ratio of the transformed MoM matrix of $\epsilon_2(x)$ after thresholding ($E_{err} = (1 \pm 0.02)\%$) as a function of the problem size using (a) the DWT, (b) the DWPT based on excitation tree, (c) the DWPT based on the row tree, (d) the DWPT based on the column tree, and (e) the DWPT based on the column and row tree.

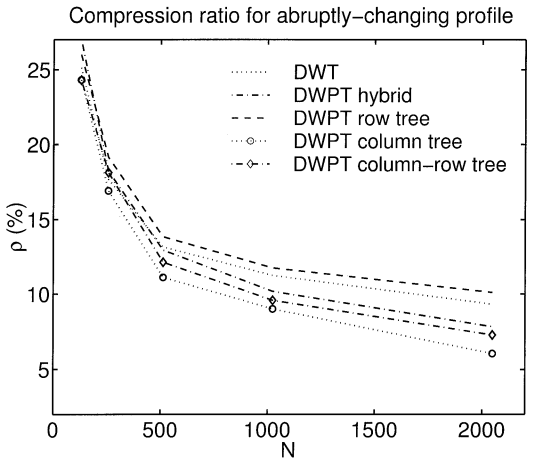

Fig. 14 The compression ratio in the transformed MoM matrix of $\epsilon_3(x)$ after thresholding ($E_{err} = (1 \pm 0.02)\%$) as a function of the problem size using (a) the DWT, (b) the DWPT based on excitation tree, (c) the DWPT based on the row tree, (d) the DWPT based on the column tree, and (e) the DWPT based on the column-row tree.

$E_{err} = (1 \pm 0.02)\%$. It is clear that the solution of the sparse matrix equation obtained by wavelet transform is faster than that of the original dense matrix equation. According to these two figures, the slope for the DWT algorithm is larger than the slope for the DWPT-based algorithms, hence the time cost of MVM will be less for large N. Note that here we did not include the CPU time required for matrix transformation and packet tree selection. These procedures may introduce significant burdens for systems with only one excitation or small N.

5. Conclusions

The wavelet algorithms have been applied to the one-dimensional dielectric scattering problems. As we expected, applying the DWT or the DWPT algorithms to the excitation-based method or the $[\boldsymbol{Z}]$-matrix-based method lead to sparse matrix equations, which have the merits of saving memory and speeding up the solution. If we want to obtain a better compression ratio of the matrix by the excitaion methods, a modified reference vector should be used. Besides, because there are no much high frequency components of the field in the dielectric region, the wavelet coefficients of the small scales components (corresponding to the high frequency components) are very small and negligible. However, it is not good if a more precise result as well as a smaller compression ratio are required simultaneously, since while reducing the MoM matrix, the elements which contain the interaction between different scales are deleted, and the deletion of these elements

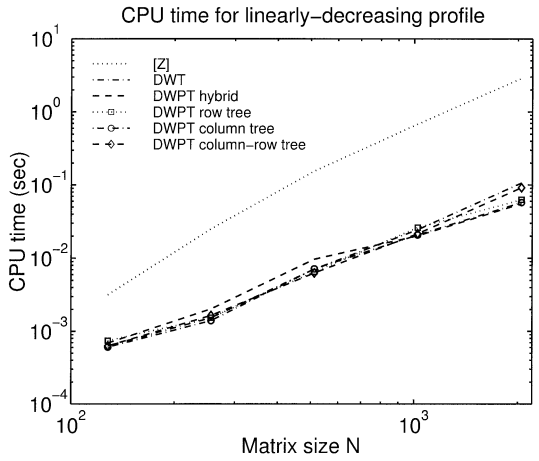

Fig. 15 CPU time required to implement the matrix-vector multiplication (MVM) as a function of problem size N. The MoM matrices corresponding to the linearly-decreasing profile are used.

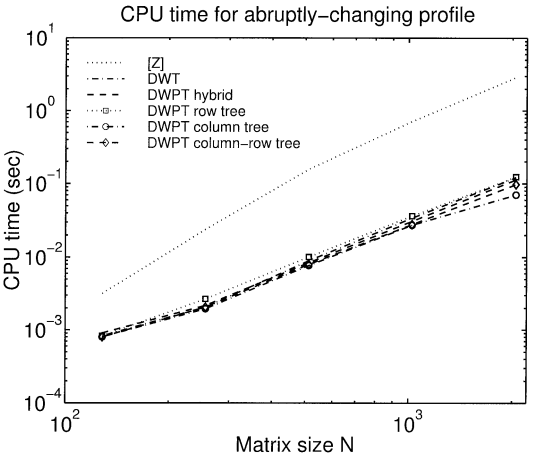

Fig. 16 CPU time required to implement the matrix-vector multiplication (MVM) as a function of problem size N. The MoM matrices corresponding to the abruptly-changing profile are used.

may lead to inaccurate results. Hence, it is inferior to the $[\boldsymbol{Z}]$-matrix-based method.

On the other hand, the $[\boldsymbol{Z}]$-matrix-based method gives better results of sparsity because the interaction between different scales are preserved. The cost is the additional computation time. Among these methods, if the DWPT-based methods are applied, the column tree will give a better basis transform owing to their completeness of decomposition. The cost of a matrix-vector multiplication for the wavelet-domain sparse matrix is reduced by a factor of 10, compared with that of the original dense matrix. Thus, for large N problems, the wavelet domain methods can be advantageous.

Of course, it is even better if we can create a sparse coefficient matrix without the similarity transform. Some studies in this direction is in progress, and hopefully will be reported soon.

References

[1] B.Z. Steinberg and Y. Leviatan, "On the use of wavelet expansions in the method of moments," IEEE Trans. Antennas Propagat., vol. 41, no. 5, pp. 610–619, May 1993.
[2] B.Z. Steinberg and Y. Leviatan, "Periodic wavelets expansions for analysis of scattering from metallic cylinders," Microwave Opt. Technol. Lett., vol.7, no.6, pp.266–268, April 1994.
[3] J.C. Goswami, A.K. Chan, and C.K. Chui, "On solving first-kind integral equations using wavelets on a bounded interval," IEEE Trans. Antennas Propagat., vol.43, no.6, pp.614–622, June 1995.
[4] G. Wang, "Application of wavelets on the interval to the analysis of thin-wire antennas," IEEE Trans. Antennas Propagat., vol.45, no.5, pp.885–893, May 1997.
[5] R.L. Wagner and W.C. Chew, "A study of wavelets for the solution of electromagnetic integral equations," IEEE Trans. Antennas Propagat., vol.43, no.8, pp.802–810, Aug. 1995.
[6] W.L. Golik, "Wavelet packets for fast solution of electromagnetic integral equation," IEEE Trans. Antennas Propagat., vol.46, no.5, pp.618–624, May 1998.
[7] H. Deng and H. Ling, "Moment matrix sparsification using adaptive wavelet packet transform," Electro. Lett., vol.33, no.13, pp.1127–1128, June 1997.
[8] H. Deng and H. Ling, "Application of adaptive wavelet packet basis to solving electromagnetic integral equations," IEEE AP-S Int. Symp. Dig., pp.1740–1743, Atlanta, Georgia, June 21–26, 1998.
[9] Z. Baharav and Y. Leviatan, "Impedance matrix compresion using adaptively constructed basis functions," IEEE Trans. Antennas Propagat., vol.44, no.9, pp.1231–1238, Sept. 1996.
[10] Z. Baharav and Y. Leviatan, "Impedance matrix compression using iterative selected wavelet basis for MFIE foumulation," Microwave Opt. Technol. Lett., vol.12, no.3, pp.506–510, June 1996.
[11] H. Kim, H. Ling, and C. Lee, "A fast moment method algorithm using spectral domain wavelet concepts," Radio Science, vol.31, pp.1253–1261, Sept.-Oct. 1996.
[12] M.V. Wickerhauser, Adapted Wavelet Analysis from Theory to Software, Boston, MA, A. K. Peters, 1994.
[13] C. Taswell, "Top-down and buttom-up tree search algorithms for selecting bases in wavelet packets transforms," Proc. of the Vilard de Lans Conference, Springer Verlag, 1995.
[14] C.H. Chen, " An integral equation formulation of the direct scattering problem for an inhomogeneous slab," IEEE Trans. Antennas Propagat., vol.26, pp.797–800, Nov. 1978.
[15] R.F. Harrington, Time Harmonic Electromagnectic Field, N.Y., McGraw-Hill, 1961.
[16] S.G. Mallat, "A theory for multiresolution signal decomposition: The wavelet representations," IEEE Trans. Pattern Anal. Mach. Intel., vol.11, pp.674–693, July 1989.
[17] I. Daubechies, Ten Lectures on Wavelets, Philadelphia, PA, Soc. Indust. Appl. Math., 1992.
[18] K. Sabetfakhri and L.P.B. Katehi, "Analysis of integrated millimeter-wave and submillimeter-wave waveguides using orthonormal wavelet expansions," IEEE Trans. Microwave Theory Tech., vol.42, no.12, pp.2412–2422, Dec. 1994.

Jeng-Long Leou was born in Taitung, Taiwan, R.O.C., on Nov. 6, 1968. He received the B.S. degree in electronic engineering from National Central University, Chung-Li, Taiwan in 1991 and the M.S. and Ph.D degrees in electrical engineering from National Taiwan University, Taipei, Taiwan in 1993 and 1999, respectively. His research interests include microwave imaging, wireless communication, electromagnectic scattering and wavelet theory.

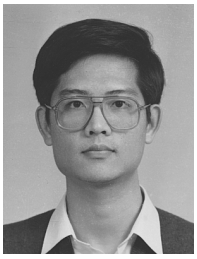

Jiunn-Ming Huang was born in Changhua, Taiwan, ROC. He received the B.Ed. degree in National Changhua University of Education, Changhua, Taiwan, in 1985, and the M.Sc. degree from Chung Chen Institute of Technology, Taoyuan, Taiwan, in 1987. He is currently pursuing the Ph.D. degree at National Chiao-Tung University, Hsinchu, Taiwan. From 1987 to 1993 he worked at Chung Shan Institute of Science and Technology(CSIST), Taoyuan, in antenna design and RCS measurements. From 1994 to 1996, he was a consultant in mobile antenna, amateur radio and RF-circuit design. His current interests include wavelets theory in scattering, computational electromagnetics and modem design.

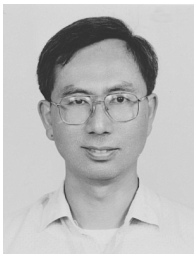

Shyh-Kang Jeng was born in I-Lan, Taiwan, R.O.C., on May 6, 1957. He received the B.S.E.E. and Ph.D. degrees from National Taiwan University, Taipei, Taiwan, R.O.C., in 1979 and 1983, respectively. In 1981, he joined the faculty of the Department of Electrical Engineering, National Taiwan University, Taipei, where he is now a Professor. From 1984 to 1985 he was an Electronic Data Processing Officer and Instructor of information system analysis and design at National Defense Management College, Chung-Ho, Taiwan. R.O.C. From 1985 to 1993, he visited University of Illinois, Urbana-Champaign, as a Visiting Research Associate Professor and a Visiting Research Professor several times. His current research interest is in three-dimensional sound, music systems, indoor and outdoor channel modeling for wireless communications, and electromagnetic scattering analysis and visualization.

Hsueh-Jyh Li was born in Yun-Lin, Taiwan, Republic of China, on August 11, 1949. He received the B.S.E.E. degree from National Taiwan University, Taipei, Taiwan, in 1971, the M.S.E.E. degree in 1980, and the Ph.D. degree from the University of Pennsylvania. Philadelphia, in 1987. Since 1973, he has been with the department of Electrical Engineering, National Taiwan University, where he is a Professor. He was with the Electro-Optics and Micorwave-Optics Laboratory of the University of Pennsylvania during the period of 1984–1987. Since August 1997, he has been the Chairman of the newly established Graduate Institute of communication Engineering at the same University. He received the Distinguished Research Award from the National Science Council, Republic of China, in 1992. His main research interests are in microstrip antennas, radar scattering, microwave imaging, radio channel characteristics and wireless communications.